

# UiO-67-type Metal–Organic Frameworks with Enhanced Water Stability and Methane Adsorption Capacity

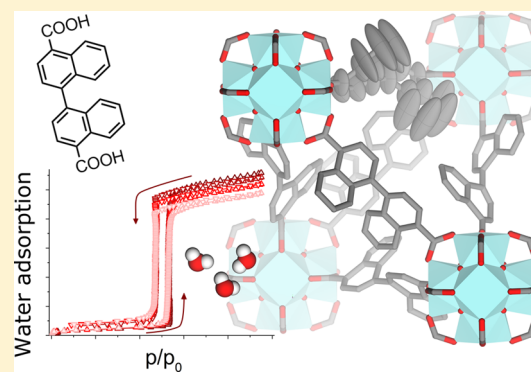
Sigurd Øien-Ødegaard,<sup>†</sup> Boris Bouchevreau,<sup>†</sup> Knut Hylland,<sup>†</sup> Lianpao Wu,<sup>†</sup> Richard Blom,<sup>‡</sup> Carlos Grande,<sup>‡</sup> Unni Olsbye,<sup>†</sup> Mats Tilset,<sup>†</sup> and Karl P. Lillerud<sup>\*,†</sup>

<sup>†</sup>Department of Chemistry, University of Oslo, P.O. Box 1033, Blindern, N-0371 Oslo, Norway

<sup>‡</sup>SINTEF, P.O. Box. 124, Blindern, N-0314 Oslo, Norway

## S Supporting Information

**ABSTRACT:** The structure and properties of two new UiO-67-type metal–organic frameworks, along with their linker synthesis and powder and single crystal synthesis, are presented. The new MOFs, UiO-67-Me and UiO-67-BN, are based on 3,3'-dimethylbiphenyl and 1,1'-binaphthyl linker scaffolds, and show a much higher stability to water than the thoroughly investigated UiO-67, which is based on the biphenyl scaffold. On the basis of structure models obtained from single crystal X-ray diffraction, it is seen that these linkers are partly shielding the Zr cluster. The new materials have higher density than UiO-67, but show a higher volumetric adsorption capacity for methane. UiO-67-BN exhibits excellent reversible water sorption properties, and enhanced stability to aqueous solutions over a wide pH range; it is to the best of our knowledge the most stable Zr-MOF that is isostructural to UiO-67 in aqueous solutions.



## INTRODUCTION

Porous metal–organic framework materials (MOFs) are currently under investigation as gas separation and storage media because of their excellent gas adsorption properties. This versatile class of materials features exceptionally high internal surface areas and ability to adsorb large amounts of gas at relatively low pressures, making them ideally suited as filling media to reduce the operating pressure of gas tanks.<sup>1</sup> With increasing worldwide consumption of natural gas, there is a growing interest for safe gas separation, storage, and transportation.<sup>2</sup>

Composed of connected inorganic clusters and organic cross-linking molecules, the materials have an intrinsic potential for diverse chemistry; the organic part (linker) can be functionalized in almost any conceivable way while the backbone remains intact. To optimize a MOF for methane storage, one strategy is to increase the heat of adsorption ( $Q_{st}$ ) by inclusion of stronger interacting sites between methane and the adsorbent.<sup>3–5</sup> Large aromatic groups on the MOF linkers, like naphthalene or anthracene, have been found to have this effect and could increase gas loading albeit inevitably also decreasing the free pore volume.<sup>6,7</sup>

The work presented herein was initially aimed at increasing the methane storage capacity of the Zr-MOF UiO-67 by increasing  $Q_{st}$  following the aforementioned strategy using linkers based on 3,3'-dimethylbiphenyl and 1,1'-binaphthyl linker scaffolds instead of the parent biphenyl. MOFs based on the Zr<sub>6</sub>-oxocluster are among the most chemically and thermally stable of the commonly investigated MOFs.<sup>8</sup> They have been synthesized with a wide variety of linkers,<sup>9</sup>

crystallizing in several topologies,<sup>10,11</sup> and some varieties have been reported to have excellent properties with respect to water adsorption and catalysis.<sup>12,13</sup> Although incorporation of bulky linkers into methane adsorbing Zr-MOFs is somewhat discouraged by Snurr et al., who found that methane packs efficiently around the Zr cluster,<sup>14</sup> it was not clear how the described effects would impact the material properties.

During the work, it became apparent that the newly synthesized MOFs were much more stable toward water than other UiO-67 analogues. Further investigations showed that UiO-67-BN was also stable during repeated water adsorption/desorption cycles. There have been several accounts on the water stability of UiO-67, and whereas it seems to be stable in water, it tends to undergo structural collapse when water is removed from an aqueous suspension.<sup>15</sup> Although adding hydrophobic groups to the linker has been demonstrated to increase MOF stability in certain cases,<sup>16</sup> this has not yet been investigated for UiO-67.

## EXPERIMENTAL SECTION

**Synthesis.** 3,3'-Dimethylbiphenyl-4,4'-dicarboxylic acid was synthesized according to our recently published method.<sup>17</sup> 1,1'-Binaphthyl-4,4'-dicarboxylic acid was synthesized using a multistep procedure described in the Supporting Information, and characterized by NMR and single crystal X-ray diffraction.

Solvothermal synthesis, based on previously reported methods in which the reagents are dissolved in DMF and heated under static

Received: October 1, 2015

conditions, was used to obtain powders and single crystals of MOFs **1**, **2**, and **3**.<sup>18,19</sup> To produce single crystals of sufficient size for single crystal X-ray diffraction, benzoic acid (for UiO-67 and UiO-67-Me) and 4-nitrobenzoic acid (for UiO-67-BN) were used as growth rate limiting additives, or “modulators”.<sup>20</sup> Powders were synthesized using less modulator, but otherwise, the conditions were similar. Both powders and single crystals were washed repeatedly with dry DMF and subsequently dry THF after synthesis. A complete description can be found in the [Supporting Information](#).

**Stability Testing.** Powders of **1**, **2**, and **3** were subjected to several chemical stability tests: suspended in aqueous solutions of pH 1, 2, 4, 10, 11, 12, 13, and 14 for 30 min (HCl(aq) and NaOH(aq), respectively); suspended in a large excess of water overnight both at 25 °C and in a sealed Teflon lined autoclave at 150 °C. Thermogravimetric analysis (TGA) was also performed on each powder sample, both as synthesized and after high temperature water treatment.

PXRD patterns were measured for the MOFs as synthesized, and following the tests. It has been reported that Zr-MOFs are prone to decompose upon evacuation of water, so PXRD measurement was performed on each sample both when dried directly from water/aqueous solution, and after solvent exchange (with THF) followed by drying. The powders were dried simply by heating in air at 200 °C, as this is sufficient to empty the pores of water, DMF, and lower boiling solvents.

**Single Crystal X-ray Diffraction.** Crystals of **2** and **3** were dried at 200 °C in air before measurement at –173 °C at the MX Beamline at the MAX2 synchrotron.<sup>21</sup> Resolution of 0.73 Å was obtained for all samples, and the structures were refined with SHELX-2015.<sup>22</sup> Following the same procedure as recently reported by us for a single crystal investigation,<sup>19</sup> the diffuse electron density of the pores was modeled with partially occupied light (dummy) atoms, which led to very good refinement indicators.

**Sorption.** Adsorption/desorption isotherms of N<sub>2</sub>, CO<sub>2</sub>, CH<sub>4</sub>, and H<sub>2</sub>O were performed on THF washed dry powders of **1**, **2**, and **3**. N<sub>2</sub> adsorption isotherms were also measured after high temperature water treatment and subsequent drying in air.

## RESULTS AND DISCUSSION

**Initial Characterization and Water Stability Test.** From PXRD measurements, it is clear that MOFs **1**, **2**, and **3** share the same crystalline phase, and similar unit cell parameters ([Figure 1](#)). All three MOFs remain structurally unchanged after dispersion in water (both at room temperature and 150 °C), if

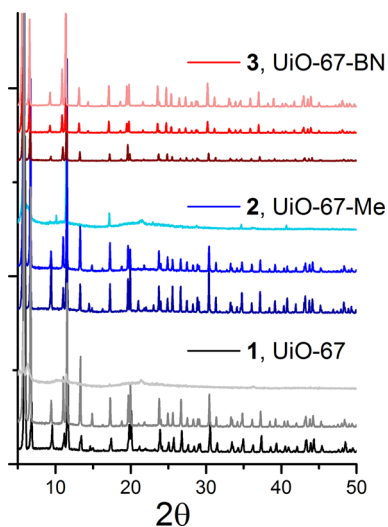


**Figure 1.** PXRD patterns of as-synthesized MOFs **1**, **2**, and **3** (dark); after water treatment at 150 °C followed by THF exchange (medium); after direct activation from water slurry (light).

water is exchanged with THF prior to solvent removal. MOFs **1** and **2** undergo structural collapse upon drying from aqueous suspension, as is expected for UiO-67, but no decomposition of **3** was observed, even after repeated dispersion and drying from liquid water. Solutions with pH ranging from 1 to 12 did not affect the crystallinity of **3**, but the material dissolved in stronger aqueous base.

BET surface areas of **1**, **2**, and **3** were obtained from measured N<sub>2</sub> isotherms using established consistency criteria,<sup>23</sup> and were found to be 2583, 1978, and 1416 m<sup>2</sup> g<sup>-1</sup>, respectively. These are in good agreement with previously reported BET surface areas for UiO-67 and with geometrical calculations (see [Supporting Information](#)). N<sub>2</sub> isotherms acquired after activation from water confirm the decomposition of **1** and **2**; following only one cycle of activation from water, sample **1** loses its porosity ( $s_A$  (BET) < 5 m<sup>2</sup> g<sup>-1</sup>), and the surface area of **2** was reduced to 1112 m<sup>2</sup> g<sup>-1</sup>. For **3**, however, only a slight increase was observed, to 1452 m<sup>2</sup> g<sup>-1</sup>. After repeated syntheses and measurements of **3** only slight deviations in  $s_A$  (BET) between as-synthesized and water-activated samples have been observed.

The newly synthesized MOFs **2** and **3** were found to be slightly less thermally stable than **1**, and started to decompose around 400 °C (see [Supporting Information](#) for TGA).

**Single Crystal Structure Analysis.** The structures of the two linkers, 1,1'-binaphthyl-4,4'-dicarboxylic acid (as a DMF solvate) and biphenyl-4,4'-dicarboxylic acid (crystal structure previously unreported of the pure compound), and MOFs **2** and **3** were characterized by single crystal X-ray diffraction. In the structure of **2** and **3**, two positions of the carboxylate oxygen were observed and allocated to missing linkers, in accordance with previous literature reports.<sup>19,24,25</sup> TGA measurements also indicate the presence of missing linker defects in the powder samples. The SC-XRD refinement statistics are summarized in [Table 1](#).

**Table 1.** Summary of Crystallographic Data for MOFs **2** and **3**

	UiO-67-Me ( <b>2</b> )	UiO-67-BN ( <b>3</b> )
space group	<i>Fm</i> $\bar{3}$ <i>m</i>	<i>Fm</i> $\bar{3}$ <i>m</i>
<i>a</i> /Å	26.8690(3)	26.8167(2)
<i>V</i> /Å <sup>3</sup>	19397.9(6)	19284.8(4)
radiation	synchrotron ( $\lambda$ = 0.750)	
2 $\theta$ range/deg	5.306–60.836	6.99–61.784
reflins	10 712	10 300
indep reflns	1290 [ $R_{int}$ = 0.0161, $R_\sigma$ = 0.0099]	1314 [ $R_{int}$ = 0.0400, $R_\sigma$ = 0.0275]
data/restraints/params	1290/0/63	1314/0/78
GOF on $F^2$	1.146	1.178
final <i>R</i> indexes [ $I \geq 2\sigma(I)$ ]	$R_1$ = 0.0349, w $R_2$ = 0.1507	$R_1$ = 0.0323, w $R_2$ = 0.0953
final <i>R</i> indexes [all data]	$R_1$ = 0.0354, w $R_2$ = 0.1515	$R_1$ = 0.0338, w $R_2$ = 0.0965
largest diff peak/hole/e Å <sup>-3</sup>	0.74/–0.56	0.64/–0.50

The crystal structures provide insight into how the carboxylate groups, and the strong adsorption sites in proximity to the Zr clusters, are influenced by the different linkers ([Figure 2](#)). In **2**, the methyl group occupies the corner of the large octahedral cage, and provides steric shielding for the carboxylate group. Its position deviates from the plane span out by the carboxylate groups (Miller plane (100)) by 18°, thus

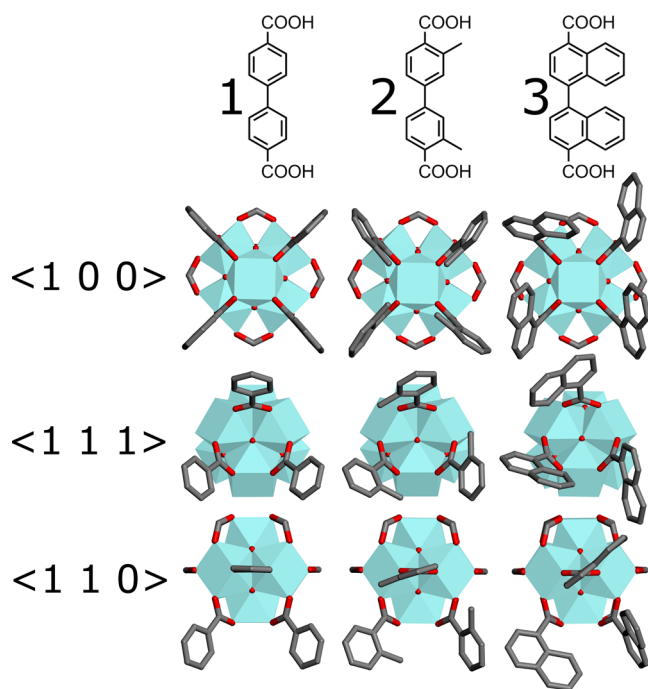


**Figure 2.** Views of the  $Zr_6$ -oxocluster environment from the [100], [111], and [110] directions reveal that the linkers sterically shield the carboxylate groups and adsorption sites on the cluster.

slightly affecting the corner of the tetrahedral cage. For 3, the effect is more pronounced: With a deviation of  $30^\circ$  from the (100) plane, the naphthyl groups are protecting both the carboxylate group and the  $\mu^3$ -O(H) group from interaction with adsorbates. At the same time, the pore volume is greatly reduced.

It is still unclear which of these structural features contribute most to the increased stability to water. While numerous functionalized UiO-67 derivatives have been reported,<sup>12,26</sup> all of these will naturally provide some steric shielding of the cluster, and reduced pore volume. It has been observed that both hydrophilic (OH functionalized UiO-67, MOF-806<sup>12</sup>) and hydrophobic (this work) groups give enhanced stability, and thus, it can be assumed that the chemical properties of the functional group are of limited importance. However, the decomposition only occurs during the evacuation of water from the MOF, which indicates that hydrolysis of the metal–linker bond is not the primary pathway of framework collapse. As previously found by Farha et al. for other Zr-MOFs, it seems the decomposition is mechanical, from capillary-like forces acting on the framework during water removal. When dried from solvents with less intermolecular interaction (i.e., less polar solvents) the framework remains intact.

The naphthyl groups of 3 sterically interact with each other, both intra- and intermolecularly, and it can be assumed they do not rotate freely. They seem however to have a significant rocking about their axis of connection, resulting in elongated thermal displacement ellipsoids. Distinction between static and dynamic conformational disorder has not yet been achieved.

In all structures, excess electron density is observed in the tetrahedral cage corners directly facing the  $\mu^3$ -O(H) group. Although the crystals are activated before measurement, they are exposed to ambient atmosphere for a few minutes before immobilization in the cryostream, during which they presumably adsorb water onto the strongest adsorption sites.

**Water Adsorption Cycles.** All four cycles of water adsorption measured on 3 at  $30^\circ\text{C}$  exhibit remarkable type IV adsorption isotherms, featuring a well-defined hysteresis loop with two virtually vertical and nearly parallel branches (Figure 3). This is generally associated with porous materials

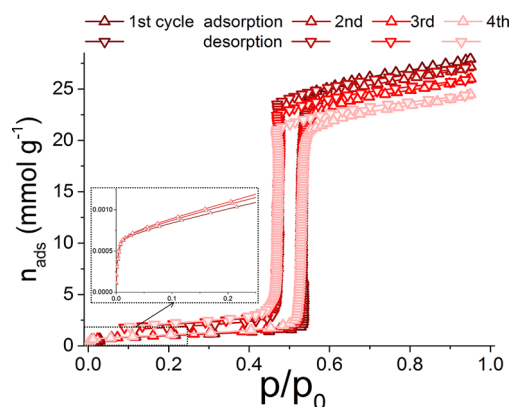


**Figure 3.** Water adsorption/desorption isotherms of 3 at  $30^\circ\text{C}$ . Inlay: The low pressure part of the adsorption isotherms magnified to show a high initial affinity to water.

having a narrow pore-size distribution. At relative humidity of 53% (at  $30^\circ\text{C}$ ) it approaches full loading of water. Although a small decrease of adsorption capacity between each cycle is observed, this is remarkable for a UiO-67-type MOF. While the cause of this decrease in capacity is unknown, it is likely connected to missing linker defects, as this has been shown to have a significant impact on Zr MOF stability,<sup>25,27,28</sup> and is present in the measured sample of UiO-67-BN. It may also be affected by the harsh regeneration between each cycle, heating the powder at  $250^\circ\text{C}$  overnight in vacuum. Further investigations of the synthesis and measurement conditions will clarify whether this is indeed the case.

The adsorption isotherm has three distinct parts; before, during, and after the water condensation. Initially ( $p/p_0 = 0.0$ – $0.4$ ), it exhibits a non-negligible rise in adsorption (for  $p/p_0 = 0.0$ – $0.02$ ), followed by a linear segment (for  $p/p_0 = 0.02$ – $0.4$ ). If we consider the crystal density of  $0.937$  for this material, the initial amount of water adsorbed ( $n_0$ ) corresponds to  $0.645$   $\text{mmol cm}^{-3}$ , or to about 7.5 water molecules per unit cell, which is in good agreement with the 8 water molecules (2 per  $Zr_6$ -cluster) expected to undergo chemisorption upon rehydroxylation of the cluster.<sup>8,29</sup> According to the Langmuir equation, more than 90% of the rehydroxylation is completed at a relative partial pressure as low as  $p/p_0 = 0.015$ .

The linear behavior (observed at  $p/p_0 = 0.02$ – $0.4$ ) of the adsorption indicates low surface coverage where the amount of adsorbate is proportional to the partial pressure, and may thus be modeled by Henry's adsorption equation. However, in order to also include the initial steep water uptake, a second contribution in the form of a Langmuir isotherm has here been added:

$$n = n_0 \frac{bp}{1 + bp} + k_H p$$

Here,  $n$  signifies the amount adsorbed at given relative pressure  $p$ ,  $n_0$  the maximum adsorption for the Langmuir-type isotherm contribution,  $b$  the Langmuir equilibrium constant (proportional to the ratio of the adsorption and desorption rate

constants), and  $k_H$  the Henry's constant characterizing the linear behavior of adsorption. The global fit over the  $p/p_0$  range 0.0–0.4 of all four isotherms gives quite satisfactory results, with a coefficient of determination  $R^2 = 0.997$ . Fitted parameters were single values for  $n_0$  and  $b$  and four individual  $k_H$  values (see Table 2).

**Table 2. Parameters Derived from the Fitting of the Low Pressure Part of the Water Adsorption Isotherms of 3 at 30 °C**

adsorption cycle	$n_0$ (mmol g <sup>-1</sup> )	$b$	$k_H$ (mol g <sup>-1</sup> Pa <sup>-1</sup> )	$\log(k_H)$
1	0.688	590	$3.63 \times 10^{-7}$	-6.44
2	0.688	590	$3.84 \times 10^{-7}$	-6.42
3	0.688	590	$4.43 \times 10^{-7}$	-6.35
4	0.688	590	$4.78 \times 10^{-7}$	-6.32

The low  $k_H$  value of 3 (average  $\log(k_H)$  of -6.4, see Table 2) suggests a hydrophobic behavior and thus limited adsorption at moderate partial water pressure ( $p/p_0 < 0.4$ ). The values reported by Canivet et al. for the parent UiO-66 and its amino-functionalized derivative have  $\log(k_H)$  values of -3.5 and -2.4, 3 and 4 orders of magnitude higher, respectively.<sup>30</sup> Among the 15 MOFs investigated by these authors, very few exhibit similar hydrophobic features; 3 is actually only comparable to the very hydrophobic ZIF-8<sup>31</sup> and to In-MIL-68<sup>32</sup> with  $\log(k_H)$  values of -6.2 and -6.6, respectively.

The second part of the adsorption isotherm consists of a water condensation phenomenon which occurs at  $p/p_0 = 0.53$  with a significant rise in water adsorption equivalent to 92% of the total water adsorption capacity. This large uptake is followed by the third part, a linear increase that could originate from further ordering of adsorbed water molecules into additional layer(s) with higher pressure, thus increasing the density in the larger pores and allowing some additional adsorption. The total water uptake finally reaches 27.4 mmol/g (0.495 cm<sup>3</sup>/g) at  $p/p_0 = 0.90$  (see Table 3).

**Table 3. Water Capacity Data Derived from Water Adsorption Isotherms at 30 °C**

MOF/ads cycle	$C_{H_2O}^*$ (cm <sup>3</sup> g <sup>-1</sup> )	no. of water molecules per unit cell
UiO-67-BN/1	0.495	299
UiO-67-BN/2	0.481	291
UiO-67-BN/3	0.461	279
UiO-67-BN/4	0.432	261
UiO-67-Me/3	0.338	172
UiO-67-Me/4	0.167	85

At  $p/p_0 = 0.50$ , just before the water condensation starts, the physisorbed water loadings range from 10 to 16 water molecules per unit cell between cycle 1 and cycle 4. At low pressure, the most favorable sites for water adsorption are at the corners of the tetrahedral cages where the capping  $\mu_3$ -O(H) groups are pointing. This means that, before the steep uptake arises, there are no more than 1–2 water molecules per tetrahedral cage on average. Although this loading is relatively small, these molecules still could take part in the formation of water microclusters around primary adsorption sites, which is generally widely accepted as the prior step to micropore filling in hydrophobic porous materials.<sup>33</sup>

The desorption branch exhibits a very similar behavior, with a slight hysteresis in water uptake all over the isotherm and an

explicit shift in pressure for the main desorption step (parallel to the adsorption one) occurring at  $p/p_0 = 0.47$ . The excess of water that is not desorbed at low pressure amounts to about 7–10 water molecules per unit cell and is possibly due to strong hydrogen bonding between those water molecules and the capping  $\mu_3$ -O(H) groups of the cluster or hydroxyl groups resulting from linker deficiency. To prevent any bias in the measurement of the ulterior adsorption isotherms, a necessary outgassing for several hours under vacuum (at  $p < 0.1$  Pa) at 250 °C was performed between each cycle.

In a comparison to those of 1 or 2, both effective pore and window sizes are reduced in 3, owing to the dimension of the extended binaphthyl linker. This gives rise to a confinement effect,<sup>34</sup> facilitating the water adsorption and thus leading to a lowering of the pore filling pressure  $\alpha$ . This effect could also be strengthened by the larger hydrophobicity of the pore walls, promoting the formation of hydrogen bonding between water molecules in such confined spaces. The pore filling pressure  $\alpha$  of UiO-67 determined from the isotherm reported by No et al. has a value of 0.56, which seems to contradict the previous assumption. However, the isotherms of the present work have been measured at 30 °C, whereas those of No et al. were measured at 25 °C. It is then worth mentioning that, as the water adsorption shifts to higher pressures with increasing temperatures, the value of pore filling pressure can change by several hundred Pascal with a 5 °C temperature variation,<sup>35</sup> eventually leading to a value of  $\alpha$  equal to or higher than 0.63 as expected at 30 °C.

The first water adsorption/desorption isotherms of both 1 and 2 were ill-defined, and few conclusions can be made with the existing data. For instance, it was not possible to determine the water adsorption capacity of the pristine materials. Whereas 1 is completely decomposed after the first cycle, 2 undergoes partial decomposition during desorption, as can be seen by a critical loss in water capacity during cycling. Yet some information, such as the adsorption capacity during cycles 3 and 4, could be extracted (see Table 3, and Figure S9 in the Supporting Information).

With the assumption that confined water has a density close to that of liquid, less than 30% of the pore volume of the pristine UiO-67 (ca. 0.98 cm<sup>3</sup>/g) is filled, considering the total uptake of about 16 mmol/g (0.288 cm<sup>3</sup>/g) reported by others.<sup>36–38</sup> On the contrary, for 3, 90% of the pore volume (0.548 cm<sup>3</sup>/g) is filled (total uptake of 0.495 cm<sup>3</sup> H<sub>2</sub>O(l) per gram at  $p/p_0 = 0.9$ ). Despite the expected larger hydrophobicity of the framework, the pore filling is here much more efficient. As already suggested for example by Cmarik et al. for the dimethoxy-functionalized UiO-66 MOF (UiO-66-2,5-(OMe)<sub>2</sub>),<sup>39</sup> in certain cases the linker is likely to be acting as a “directing agent”, implying a much more efficient packing of the water molecules.

**CH<sub>4</sub> and CO<sub>2</sub> Adsorption.** Cavka et al. reported high pressure CH<sub>4</sub> and CO<sub>2</sub> isotherms for 1 up to 80 and 30 bar, respectively, at 25, 40, and 70 °C. Analogous data for 2 and 3 are reported here (except at 70 °C for 2). To better correlate the effects of linker functionalization on the gas adsorption, isotherms are also reported with volumetric uptakes (rescaled using the crystal density of the materials).

The CH<sub>4</sub> adsorption capacity (Table 4), derived from isotherms at 25 °C (Figure 4), is moderate for all three MOFs, and below the best performing MOFs.<sup>40</sup> Despite the steric shielding of the cluster corners (which are the preferred gas adsorption sites)<sup>14</sup> and above all the reduction of porosity (by

**Table 4. Adsorption Uptakes of CH<sub>4</sub> and Working Capacities (Considering Desorption at 5 bar) at Room Temperature for 1, 2, and 3<sup>a</sup>**

	P = 35 bar		P = 65 bar	
	uptake	working capacity	uptake	working capacity
UiO-67	102	72	127	104
UiO-67-Me	113	75	135	104
UiO-67-BN	124	72	147	104

<sup>a</sup>Volumes are given in cm<sup>3</sup>(STP) cm<sup>-3</sup>.

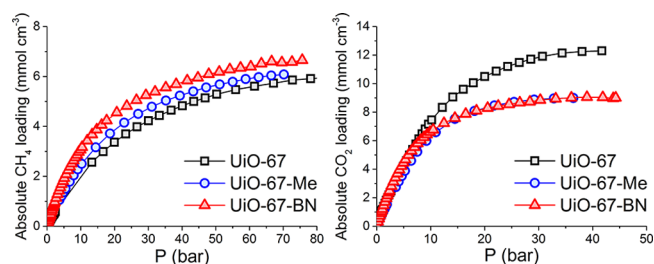


**Figure 4.** Adsorption isotherms acquired at 25 °C, showing the volumetric loading. Left: CH<sub>4</sub>. Right: CO<sub>2</sub>.

26% in the case of 3), the volumetric capacity of 3 is 147 cm<sup>3</sup>(STP) cm<sup>-3</sup> at 65 bar, whereas it is 127 for 1 and 135 for 2. This observation seems to encourage the adopted strategy of functionalizing the linker with pending methyl or aryl groups to enhance the interaction with the framework and thus the methane adsorption capacity.

However, in our case, the isosteric heat of adsorption (at zero coverage, see Table 5) increases as well with the functionaliza-

**Table 5. Heats of Adsorption (kJ mol<sup>-1</sup>) Calculated by Extrapolation of the Low Pressure Data of the Virial Isotherms ( $n$  vs  $\ln(p/n)$ )<sup>41</sup> for 1 and 3 at 25, 40, and 70 °C**

	CH <sub>4</sub>	CO <sub>2</sub>
UiO-67	15.2	23.6
UiO-67-BN	20.3	20.6

tion of the linker, leading to a non-negligible uptake at low pressure, thus rather limiting the working capacity (considering that the first 5 bar of methane pressure cannot be used in current vehicle applications). One should yet notice that the improved adsorption efficiency compensates very elegantly for the loss of pore volume over this MOF series since the working capacity at both 35 and 65 bar is surprisingly similar for the three MOFs investigated.

The volumetric isotherms of CO<sub>2</sub> adsorption (Figure 4) show as expected a significant decrease of the uptake through the MOF series, in line with the reduction of the pore volume. By physical volume only, an even more pronounced decrease in adsorption capacity would have been expected for 3 compared to 1 and 2. On the contrary, it exhibits a behavior very similar to 2 at moderate and high pressures. Thus, the packing of CO<sub>2</sub> molecules is improved in this more confined space, as was the case for water adsorption.

## CONCLUSIONS

It has been found that UiO-67-BN shows exceptional stability to aqueous solutions over a wide pH range, and to water vapor in repeated adsorption/desorption cycles. This microporous

MOF displays type IV hysteresis in water adsorption/desorption, typically associated with capillary condensation in narrow uniform pores in mesoporous materials. UiO-67-BN retains its structure when dried from an aqueous suspension, conditions in which UiO-67 collapses. From single crystal structure determination, it has been observed that the functional linkers partially shield the strongest adsorption sites of the MOFs. This steric shielding, along with reduction in pore volume, may account for the enhanced stability. CH<sub>4</sub> heat of adsorption increases when the linker is functionalized, and UiO-67-BN has a higher volumetric loading than UiO-67, despite the greatly reduced pore volume.

## ASSOCIATED CONTENT

### Supporting Information

The Supporting Information is available free of charge on the ACS Publications website at DOI: 10.1021/acs.inorgchem.5b02257. The crystal structures are submitted to The Cambridge Crystallographic Data Centre with identifiers CCDC 1422388–1422393 and can be obtained free of charge from <http://www.ccdc.cam.ac.uk/cgi-bin/catreq.cgi>. See DOI: 10.1039/x0xx00000x.

Crystal details for biphenyl-4,4'-dicarboxylic acid (CIF)

Crystal details for UiO-67-BN (CIF)

Crystal details for UiO-67-BN (SQUEEZE) (CIF)

Crystal details for 1,1'-binaphthyl-4,4'-dicarboxylic acid (CIF)

Synthesis and NMR characterization of 1,1'-binaphthyl-4,4'-dicarboxylic acid; single crystal characterization of linkers; MOF synthesis details; summary on MOF single crystal X-ray diffraction; thermogravimetric analysis (TGA); surface area calculations; N<sub>2</sub> adsorption; high pressure CO<sub>2</sub> and CH<sub>4</sub> sorption methods (PDF)

Crystal details for UiO-67-Me (CIF)

Crystal details for UiO-67-Me (SQUEEZE) (CIF)

## AUTHOR INFORMATION

### Corresponding Author

\*E-mail: [k.p.lillerud@kjemi.uio.no](mailto:k.p.lillerud@kjemi.uio.no).

### Author Contributions

The manuscript was written through contributions of all authors. All authors have given approval to the final version of the manuscript.

### Notes

The authors declare the following competing financial interest(s): K.P. Lillerud and U. Olsbye have a financial interest in the start-up company ProfMOF A/S, which is seeking to commercialize metal–organic frameworks.

## ACKNOWLEDGMENTS

This work is part of CLIMIT and FutureFeedstock, which receives financial support from the Research Council of Norway under Contracts 215735 and 228157, respectively. The authors would like to thank the staff at beamline I911-3 at MaxLAB for their support at the beamline.

## REFERENCES

- (1) Service, R. F. *Science* **2014**, *346*, 538–541.
- (2) Wang, Q.; Chen, X.; Jha, A. N.; Rogers, H. *Renewable Sustainable Energy Rev.* **2014**, *30*, 1–28.
- (3) Getman, R. B.; Bae, Y. S.; Wilmer, C. E.; Snurr, R. Q. *Chem. Rev.* **2012**, *112*, 703–723.

- (4) Mason, J. A.; Veenstra, M.; Long, J. R. *Chem. Sci.* **2014**, *5*, 32–51.
- (5) Lee, S.-J.; Bae, Y.-S. *J. Phys. Chem. C* **2014**, *118*, 19833–19841.
- (6) Ma, S.; Sun, D.; Simmons, J. M.; Collier, C. D.; Yuan, D.; Zhou, H.-C. *J. Am. Chem. Soc.* **2008**, *130*, 1012–1016.
- (7) Düren, T.; Sarkisov, L.; Yaghi, O. M.; Snurr, R. Q. *Langmuir* **2004**, *20*, 2683–2689.
- (8) Cavka, J. H.; Jakobsen, S.; Olsbye, U.; Guillou, N.; Lamberti, C.; Bordiga, S.; Lillerud, K. P. *J. Am. Chem. Soc.* **2008**, *130*, 13850–13851.
- (9) Kim, M.; Cohen, S. M. *CrystEngComm* **2012**, *14*, 4096–4104.
- (10) Liu, T.-F.; Feng, D.; Chen, Y.-P.; Zou, L.; Bosch, M.; Yuan, S.; Wei, Z.; Fordham, S.; Wang, K.; Zhou, H.-C. *J. Am. Chem. Soc.* **2015**, *137*, 413–419.
- (11) Bon, V.; Senkovskyy, V.; Senkovska, I.; Kaskel, S. *Chem. Commun.* **2012**, *48*, 8407–8409.
- (12) Furukawa, H.; Gandara, F.; Zhang, Y.-B.; Jiang, J.; Queen, W. L.; Hudson, M. R.; Yaghi, O. M. *J. Am. Chem. Soc.* **2014**, *136*, 4369–4381.
- (13) Wang, C.; Xie, Z.; deKrafft, K. E.; Lin, W. *J. Am. Chem. Soc.* **2011**, *133*, 13445–13454.
- (14) Gomez-Gualdron, D. A.; Gutov, O. V.; Krungleviciute, V.; Borah, B.; Mondloch, J. E.; Hupp, J. T.; Yildirim, T.; Farha, O. K.; Snurr, R. Q. *Chem. Mater.* **2014**, *26*, 5632–5639.
- (15) Mondloch, J. E.; Katz, M. J.; Planas, N.; Semrouni, D.; Gagliardi, L.; Hupp, J. T.; Farha, O. K. *Chem. Commun.* **2014**, *50*, 8944–8946.
- (16) Burtch, N. C.; Jasuja, H.; Walton, K. S. *Chem. Rev.* **2014**, *114*, 10575–10612.
- (17) Hylland, K. T.; Øien-Ødegaard, S.; Lillerud, K. P.; Tilset, M. *Synlett* **2015**, *26*, 1480–1485.
- (18) Schaate, A.; Roy, P.; Godt, A.; Lippke, J.; Waltz, F.; Wiebcke, M.; Behrens, P. *Chem. - Eur. J.* **2011**, *17*, 6643–6651.
- (19) Øien, S.; Wragg, D.; Reinsch, H.; Svelle, S.; Bordiga, S.; Lamberti, C.; Lillerud, K. P. *Cryst. Growth Des.* **2014**, *14*, 5370–5372.
- (20) Tsuruoka, T.; Furukawa, S.; Takashima, Y.; Yoshida, K.; Isoda, S.; Kitagawa, S. *Angew. Chem., Int. Ed.* **2009**, *48*, 4739–4743.
- (21) Ursby, T.; Unge, J.; Appio, R.; Logan, D. T.; Fredslund, F.; Svensson, C.; Larsson, K.; Labrador, A.; Thunnissen, M. M. G. M. *J. Synchrotron Radiat.* **2013**, *20*, 648–653.
- (22) Sheldrick, G. *Acta Crystallogr., Sect. C: Struct. Chem.* **2015**, *71*, 3–8.
- (23) Sing, K. S. W. In *Adsorption by Powders and Porous Solids*, 2nd ed.; Rouquerol, F., Rouquerol, J., Sing, K. S. W., Llewellyn, P., Maurin, G., Eds.; Academic Press: Oxford, 2014; pp 237–268.
- (24) Trickett, C. A.; Gagnon, K. J.; Lee, S.; Gandara, F.; Bürgi, H.-B.; Yaghi, O. M. *Angew. Chem., Int. Ed.* **2015**, *54*, 11162–11167.
- (25) Shearer, G. C.; Chavan, S.; Ethiraj, J.; Vitillo, J. G.; Svelle, S.; Olsbye, U.; Lamberti, C.; Bordiga, S.; Lillerud, K. P. *Chem. Mater.* **2014**, *26*, 4068–4071.
- (26) Katz, M. J.; Brown, Z. J.; Colon, Y. J.; Siu, P. W.; Scheidt, K. A.; Snurr, R. Q.; Hupp, J. T.; Farha, O. K. *Chem. Commun.* **2013**, *49*, 9449–9451.
- (27) Wu, H.; Chua, Y. S.; Krungleviciute, V.; Tyagi, M.; Chen, P.; Yildirim, T.; Zhou, W. *J. Am. Chem. Soc.* **2013**, *135*, 10525–10532.
- (28) Ghosh, P.; Colon, Y. J.; Snurr, R. Q. *Chem. Commun.* **2014**, *50*, 11329–11331.
- (29) Valenzano, L.; Civalieri, B.; Chavan, S.; Bordiga, S.; Nilsen, M. H.; Jakobsen, S.; Lillerud, K. P.; Lamberti, C. *Chem. Mater.* **2011**, *23*, 1700–1718.
- (30) Canivet, J.; Bonnefoy, J.; Daniel, C.; Legrand, A.; Coasne, B.; Farrusseng, D. *New J. Chem.* **2014**, *38*, 3102–3111.
- (31) Park, K. S.; Ni, Z.; Cote, A. P.; Choi, J. Y.; Huang, R.; Uribe-Romo, F. J.; Chae, H. K.; O’Keeffe, M.; Yaghi, O. M. *Proc. Natl. Acad. Sci. U. S. A.* **2006**, *103*, 10186–10191.
- (32) Volkringer, C.; Meddouri, M.; Loiseau, T.; Guillou, N.; Marrot, J.; Férey, G.; Haouas, M.; Taulelle, F.; Audebrand, N.; Latroche, M. *Inorg. Chem.* **2008**, *47*, 11892–11901.
- (33) Brennan, J. K.; Bandoz, T. J.; Thomson, K. T.; Gubbins, K. E. *Colloids Surf., A* **2001**, *187–188*, 539–568.
- (34) Gor, G. Y.; Rasmussen, C. J.; Neimark, A. V. *Langmuir* **2012**, *28*, 12100–12107.
- (35) Alcañiz-Monge, J.; Linares-Solano, A.; Rand, B. J. *Phys. Chem. B* **2001**, *105*, 7998–8006.
- (36) DeCoste, J. B.; Peterson, G. W.; Jasuja, H.; Glover, T. G.; Huang, Y.-g.; Walton, K. S. *J. Mater. Chem. A* **2013**, *1*, 5642–5650.
- (37) Jeremias, F.; Frohlich, D.; Janiak, C.; Henninger, S. K. *New J. Chem.* **2014**, *38*, 1846–1852.
- (38) Ko, N.; Hong, J.; Sung, S.; Cordova, K. E.; Park, H. J.; Yang, J. K.; Kim, J. *Dalton Trans.* **2015**, *44*, 2047–2051.
- (39) Cmarik, G. E.; Kim, M.; Cohen, S. M.; Walton, K. S. *Langmuir* **2012**, *28*, 15606–15613.
- (40) He, Y.; Zhou, W.; Qian, G.; Chen, B. *Chem. Soc. Rev.* **2014**, *43*, 5657–5678.
- (41) Talu, O. *Adv. Colloid Interface Sci.* **1998**, *76–77*, 227–269.